ELSEVIER

Cardiovascular Research 42 (1999) 477–489

Cardiovascular Research

Ionic targets for drug therapy and atrial fibrillation-induced electrical remodeling: insights from a mathematical model

Marc Courtemanche[a,b,*], Rafael J. Ramirez[a], Stanley Nattel[a,c,d]

[a]*Research Center, Montreal Heart Institute, 5000 Bélanger, Montréal, QC H1T 1C8, Canada*
[b]*Département de Physiologie, Université de Montréal, Montréal, QC H3C 3J7, Canada*
[c]*Department of Pharmacology, McGill University, Montreal, QC H3G 1Y6, Canada*
[d]*Département de Médecine, Université de Montréal, Montréal, QC H3C 3J7, Canada*

Received 21 September 1998; accepted 28 December 1998

Abstract

Recent advances in molecular electrophysiology have made possible the development of more selective ion channel blockers for therapeutic use. However, more information is needed about the effects of blocking specific channels on repolarization in normal human atrium and in atrial cells of patients with atrial fibrillation (AF). AF-induced electrical remodeling is associated with reductions in transient outward current (I_{to}), ultrarapid delayed rectifier current (I_{Kur}), and L-type calcium current ($I_{Ca,L}$). Direct evaluation of the results of ion channel depression is limited by the nonspecificity of the available pharmacological probes. **Objectives:** Using a mathematical model of the human atrial action potential (AP), we aimed to: (1) evaluate the role of ionic abnormalities in producing AP changes characteristic of AF in humans and (2) explore the effects of specific channel blockade on the normal and AF-modified AP (AFAP). **Methods:** We used our previously developed mathematical model of the normal human atrial AP (NAP) based on directly measured currents. We constructed a model of the AFAP by incorporating experimentally-measured reductions in I_{to} (50%), I_{Kur} (50%), and $I_{Ca,L}$ (70%) current densities observed in AF. **Results:** The AFAP exhibits the reductions in AP duration (APD) and rate-adaption typical of AF. The reduction in $I_{Ca,L}$ alone can account for most of the morphological features of the AFAP. Inhibition of I_{to} by 90% leads to a reduction in APD measured at −60 mV in both the NAP and AFAP. Inhibition of the rapid component of the delayed rectifier (I_{Kr}) by 90% slows terminal repolarization of the NAP and AFAP and increases APD by 38% and 34%, respectively. Inhibition of I_{Kur} by 90% slows early repolarization and increases plateau height, activating additional I_K and causing no net change in APD at 1 Hz in the NAP. In the presence of AF-induced ionic modifications, I_{Kur} inhibition increases APD by 12%. Combining I_{Kur} and I_{Kr} inhibition under both normal and AF conditions synergistically increases APD. In the NAP, altering the model parameters to reproduce other typical measured AP morphologies can significantly alter the response to K^+-channel inhibition. **Conclusions:** (1) The described abnormalities in I_{to}, I_{Kur} and $I_{Ca,L}$ in AF patients can account for the effects of AF on human AP properties; (2) AP prolongation by I_{Kur} block is limited by increases in plateau height that activate more I_K; (3) Blockers of I_{Kur} may be more effective in prolonging APD in patients with AF; 4) Inhibition of both I_{Kur} and I_{Kr} produces supra-additive effects on APD. These observations illustrate the importance of secondary current alterations in the response of the AP to single channel blockade, and have potentially important implications for the development of improved antiarrhythmic drug therapy for AF.

Keywords: Experimental; Heart; Cellular; Human; Electrophysiology; Arrhythmia mechanisms; Computer modeling; Membrane currents; Atrial fibrillation

1. Introduction

Atrial fibrillation (AF) is self-perpetuating in nature [1], suggesting that the arrhythmia causes electrophysiological modifications that may contribute to the maintenance of the disease. Recent studies have shown that AF induces significant changes in the electrophysiological properties of atrial tissue that promote AF initiation and maintenance, and that these changes are due to atrial tachycardia [1,2]. This electrical remodeling includes shortening of the

*Corresponding author. Tel.: +1-514-376-3330 extn. 3490; fax: +1-514-376-1355.
E-mail address: msc@icm.umontreal.ca (M. Courtemanche)

Time for primary review 31 days.

0008-6363/99/$ – see front matter
PII: S0008-6363(99)00034-6

effective refractory period (ERP) [1,3–7], abbreviation of the action potential (AP) [8], decreased shortening of ERP and AP duration (APD) usually associated with increases in stimulation rate (rate-adaptation) [1,3,6–8], and increased dispersion of cellular refractoriness [9–11]. Vulnerability to AF in man has been linked to decreased rate-adaptation of the refractory period [12], pointing to the potential clinical importance of remodeling-induced reductions in ERP rate-adaptation. Tachycardia-induced remodeling has been shown to promote AF maintenance via reductions in excitation wavelength and increases in the dispersion of refractoriness that promote multiple-wavelet reentry [6,11].

A variety of changes in ionic currents have been described in atrial myocytes from animals and humans with AF or with maintained atrial tachycardia at rates similar to those of AF. In an experimental dog model, right atrial pacing at 400 bpm was shown to progressively reduce the transient outward potassium current (I_{to}) and L-type calcium current ($I_{Ca,L}$) [8]. The results of pharmacological interventions suggest that tachycardia-induced reductions in APD and APD rate-adaptation in dogs are largely due to $I_{Ca,L}$ reduction [8]. Studies of atrial tissue samples from patients with AF show similar reductions in atrial APD and rate-adaptation [9]. Recent work on isolated human atrial myocytes has shown that I_{to} and the ultrarapid delayed rectifier current (I_{Kur}), linked to the cloned Kv1.5 channels, are reduced in patients with AF [10]. Preliminary studies also show a reduction in $I_{Ca,L}$ [13] of the same order as that observed in dogs with chronic atrial tachycardia [8].

It is presently unclear whether the ionic abnormalities observed in clinical and experimental models of AF can account for the observed differences between the ''normal'' AP (NAP) recorded in atrial myocytes from patients in sinus rhythm and the ''AF-modified'' AP (AFAP) recorded in cells from patients in chronic AF. The respective roles of the observed ionic abnormalities in producing the AFAP changes are also uncertain. Previous attempts to address these issues have used pharmacological probes [8], all of which have problems with limited specificity and potentially complex voltage- and time-dependent action. In addition, it is unclear to what extent AF-induced alterations in AP morphology can modify the response of the AP to K^+-current inhibition. The effects of channel-specific K^+-current inhibition on the NAP and AFAP are relevant because these currents are possible ionic targets for drug therapy in AF. Some of these currents are already targets for existing drug therapies, but the pharmacological agents currently in use are usually not specific to a single ionic channel. In the present manuscript, we address these issues using an alternative approach based on a mathematical model of the normal human atrial AP [14] that includes specific formulations of ionic currents based on direct measurements in atrial myocytes. The model is used to investigate the effects of AF-induced ion channel modifications on the AP with the following objectives: (1) to determine whether the ionic current abnormalities reported in myocytes from patients with AF account for the observed AFAP changes; (2) to assess the relative importance of individual ionic currents to the overall AFAP changes; (3) to determine how normal AP morphological heterogeneity and the ionic abnormalities caused by AF alter the response of the atrial AP to specific ionic current inhibition.

2. Methods

The NAP model is implemented as described in Courtemanche et al. [14]. A schematic diagram of the model cell including currents, pumps, exchangers and cellular compartments is given in Fig. 1. The cell membrane is modelled electrically as a capacitor connected in parallel with variable resistances and batteries representing the ionic channels and driving forces. The time derivative of the membrane potential V (assuming an equipotential cell) is then given by

$$\frac{dV}{dt} = \frac{-(I_{ion} + I_{st})}{C_m} \quad (1)$$

where I_{ion} and I_{st} are the total ionic current and stimulus current flowing across the membrane and C_m is the total membrane capacitance. The total ionic current is given by

$$I_{ion} = I_{Na} + I_{K1} + I_{to} + I_{Kur} + I_{Kr} + I_{Ks} + I_{Ca,L} + I_{p,Ca} + I_{NaK} + I_{NaCa} + I_{b,Na} + I_{b,Ca} \quad (2)$$

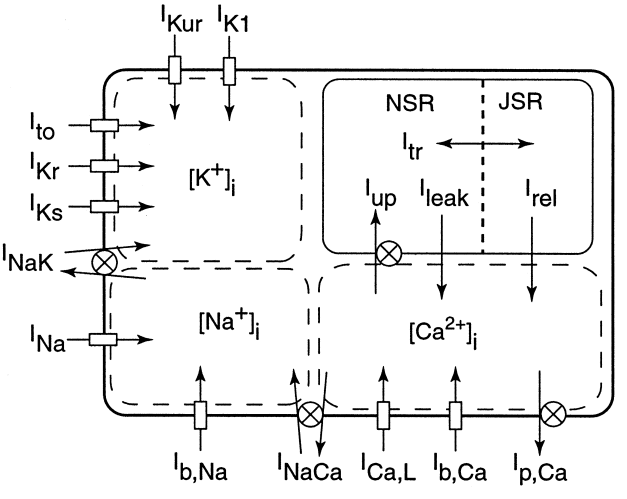

Fig.1. Schematic representation of the model cell. Sarcolemmal membrane channels are depicted using small rectangles across the cell membrane. The ionic species flowing across the channel is identified by the intracellular pool (dashed intracellular compartment) into which it flows. Pumps and exchangers are depicted using a circular symbol with a centered ''×''. The sarcoplasmic reticulum (SR, the solid intracellular compartment) is divided into two compartments: the SR release compartment or junctional SR (JSR), and the SR uptake compartment or network SR (NSR).

The total ionic current includes contributions from the fast sodium current (I_{Na}), the inward rectifier potassium current (I_{K1}), I_{to}, I_{Kur}, the rapid classical delayed rectifier potassium current (I_{Kr}), the slow classical delayed rectifier potassium current (I_{Ks}), $I_{Ca,L}$, a sarcolemmal calcium pump current ($I_{p,Ca}$), the sodium–potassium pump current (I_{NaK}), the sodium–calcium exchanger current (I_{NaCa}), a background sodium current ($I_{b,Na}$) and a background calcium current ($I_{b,Ca}$). A detailed description of all ionic and pump currents, along with a complete listing of parameter values and the detailed equations describing the handling of intracellular calcium ($[Ca^{2+}]_i$) by the sarcoplasmic reticulum system can be found in Ref. [14]. The model keeps track of the intracellular concentrations of sodium, calcium, and potassium. No extracellular cleft spaces are included in the model (extracellular ion concentrations are fixed). The total membrane capacitance is taken to be 100 (picofarads) pF. Unless otherwise noted, physical units are as follows: time is in milliseconds (ms), membrane potential is in millivolts (mV), membrane capacitance is in pF, current density is in picoamperes per pF (pA/pF), conductance is in nanosiemens per pF (nS/pF), and concentrations are in millimoles per liter (mM).

The AFAP model is implemented by incorporating experimentally-measured ionic current density reductions into our original NAP model. Among the candidate currents for a role in AF-induced electrical remodeling are I_{to}, I_{Kur} and $I_{Ca,L}$. These currents have been studied in both normal and AF-altered or atrial tachycardia-altered myocytes. In chronic AF, human atrial I_{to} and I_{Kur} conductances were found to be approximately halved compared to cells from patients in normal sinus rhythm [10]. In human atrial cells from patients with chronic AF, $I_{Ca,L}$ amplitude was reduced by about 70% compared to patients in normal sinus rhythm [13]. Similar results were observed in canine atrial cells: voltage- and time-dependent properties of $I_{Ca,L}$ remained at control levels after up to 42 days of rapid pacing, while current density was progressively attenuated (about 70% reduction after 42 days) [8].

Based on the available data, we chose to model the AFAP by implementing the experimentally-measured reductions in maximal current densities through decreases in the maximal conductances of the currents in the model: 50% reduction in the maximal conductance of I_{to}, 50% reduction in the maximal conductance of I_{Kur}, and 70% reduction in the maximal conductance of $I_{Ca,L}$. Except for these specific maximal conductance changes, the AFAP model is identical to our original NAP model [14]. Both the NAP and AFAP models are used to carry out simulations in the remainder of this study, with the results of specific channel inhibition modeled by reducing the density of the corresponding current without altering its kinetic or voltage-dependent properties.

Numerical integration of Eq. (2) is carried out using a modified Euler method with a fixed time step $\Delta t = 0.005$ ms (see Appendix in Ref. [14]). All simulations were performed on local unix workstations using double-precision arithmetic.

Model APD is measured as the time spent above -60 mV (APD_{-60}). We selected this measure for its ease of calculation, the fact that it does not depend on the amount of AP overshoot into positive potentials, and the fact that cellular excitability normally returns in the range of -60 mV. However, since the available experimental data on rate-dependence of the APD is based on the time to 90% repolarization (APD_{90}), we have used APD_{90} for direct comparison to experimental data in Section 3.2. All AP simulation results are presented after 12 s of pacing from rest. As pointed out in Ref. [14], the model parameters are adjusted to produce stable ionic concentrations at rest, i.e., in the absence of stimulation. Under periodic stimulation, there are two phases of model AP adaptation to pacing rate: the first is a relatively rapid adaptation due to the kinetic properties of the current gating variables, while the second is a slow adaptation due to drift of intracellular ionic concentrations. Twelve seconds of pacing is sufficient to ensure rapid rate-adaptation of the AP. For example, upon stimulation from rest at a period of 300 ms, the AP initially displays an alternation of long and short durations that subsides after about 10 s of pacing. Further slow decreases in APD can take up to 20 min to develop in the model. This is not unique to our model and is commonly observed in ionic models that attempt to dynamically track intracellular ionic concentrations [15]. Although such slow changes are known to occur experimentally, in the model they clearly depend on the nature of the stimulus used and on the ionic species assumed to carry the stimulus charge. The necessary careful investigation of these long-term changes in ionic models has not yet been performed in the present or other models. Because of this, we did not wish to include these very slow effects in our results and chose to present simulations after 12 s of pacing, at which point rapid rate-adaptation of the AP is complete.

3. Results

3.1. The model NAP and AFAP

Fig. 2 compares the membrane potential profiles of the model NAP and AFAP along with the major ionic currents underlying their morphology. A detailed analysis of the properties of our NAP model can be found in Ref. [14]. The second panel from the top of Fig. 2 highlights the interplay between I_{to}, I_{Kur}, and $I_{Ca,L}$ during the APs. The reductions implemented in the AFAP model for these three currents are clearly apparent when the current profiles are compared to those of the NAP model. The shorter duration and triangular morphology of the AFAP is associated with reduced I_{Kr}, I_{Ks}, and I_{NaCa} exchanger current amplitudes, as shown in the third panel of Fig. 2. The fourth and fifth

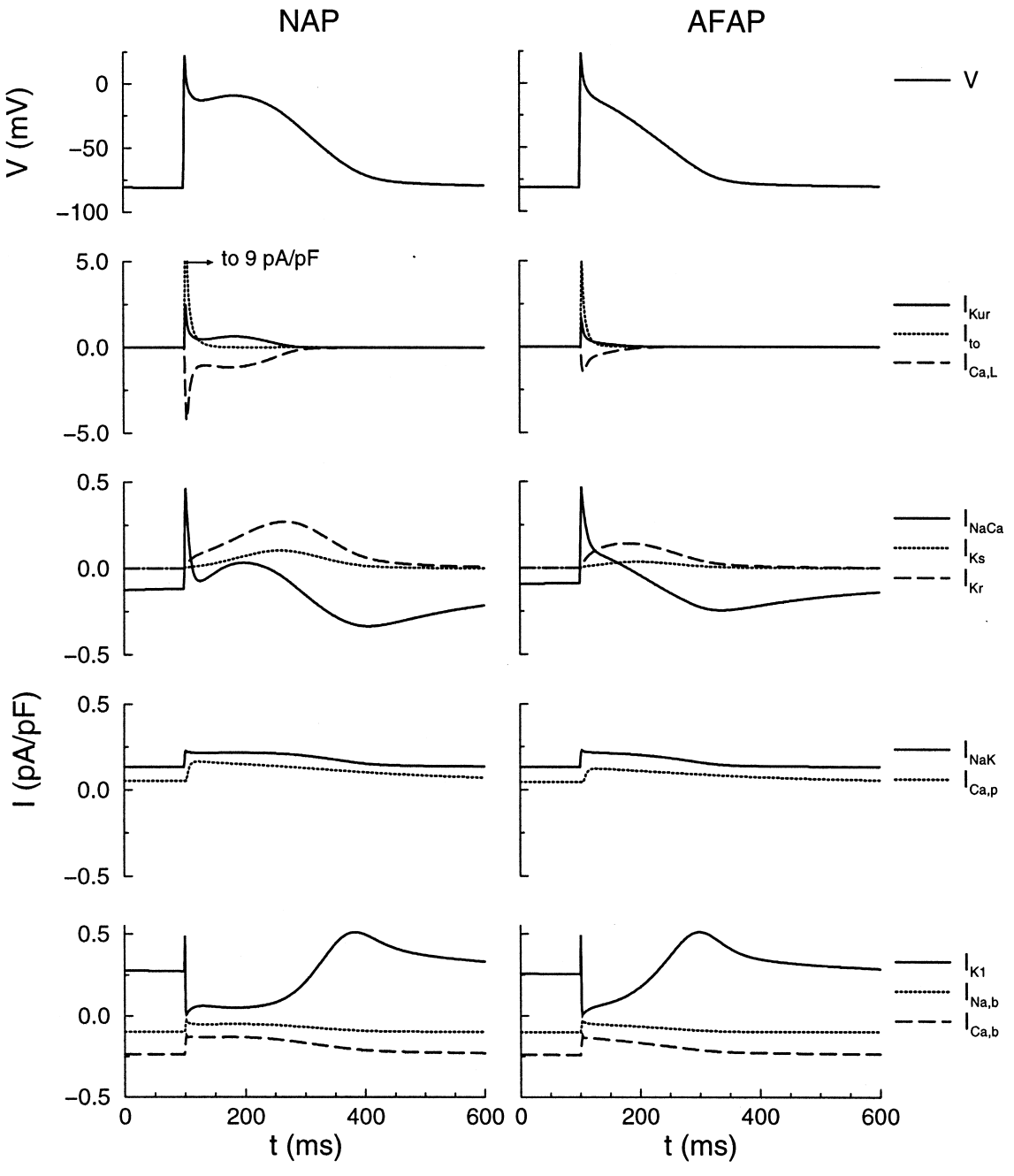

Fig. 2. Model action potentials and underlying ionic currents. Membrane potential and corresponding ionic currents are shown for the model NAP (left) and AFAP (right). The models were stimulated from rest at a period of 1000 ms. Model output from the 12th action potential is depicted. The NAP I_{to} current peaks off the graph scale at 9 pA/pF, as indicated.

panels of Fig. 2 show that the pump currents, I_{K1}, and the background currents exhibit similar profiles in the NAP and AFAP.

The respective morphologies of the model NAP and AFAP are compared with experimentally-recorded APs from patients in sinus rhythm and in chronic AF in Fig. 3. Experimental APs from Boutjidir et al. [9] were digitized and reproduced. There is good agreement between AF-induced changes in the model and experimentally-recorded APs, suggesting that the ionic current abnormalities reported in myocytes from patients with AF can account for the observed AFAP morphology when incorporated into the model.

In order to assess the relative importance of individual ionic currents in producing the overall AFAP changes, we investigated the morphological response of the model NAP to individual AF-induced alterations in I_{to}, I_{Kur}, and $I_{Ca,L}$ current densities. The top left panel of Fig. 4 reproduces the comparison of the model NAP and AFAP. Successive panels show a comparison between the model NAP and

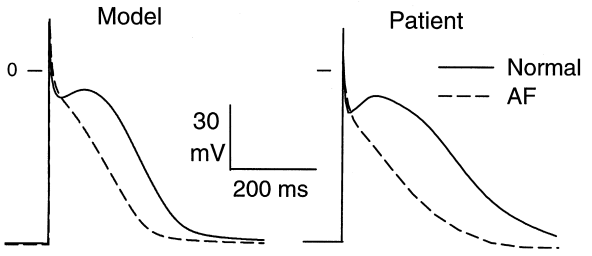

Fig. 3. Comparison of model APs (left) with experimentally recorded APs from tissue samples of patients (right). In each panel, both NAP (solid line) and AFAP (dashed line) morphologies are compared. Experimental data is adapted from Boutjidir et al. [9].

APs with only one of I_{to} (lower left), I_{Kur} (lower right), or $I_{Ca,L}$ (upper right) currents altered in the same way as in the AFAP. The effects of individual current abnormalities on the NAP reveal that $I_{Ca,L}$ reduction plays the major role in the observed change between the model NAP and AFAP, reproducing the triangular morphology and abbreviation of the AP typical of AF. Compared to the AP with $I_{Ca,L}$ alteration alone, the reductions in I_{to} and I_{Kur} produce a slowing of phase 1 repolarization and an increase in AP plateau height that may play a role in modulating the response of the AFAP to potassium current inhibition (see below).

3.2. Rate-adaptation

A shortened APD and decreased adaptation to rate have been observed as a consequence of AF-induced remodeling [9,16]. We investigated the rate-dependence of APD measured at APD_{90} in both NAP and AFAP. Fig. 5 illustrates the relationship between APD_{90} and basic pacing cycle length for the model NAP and AFAP (left panel) and

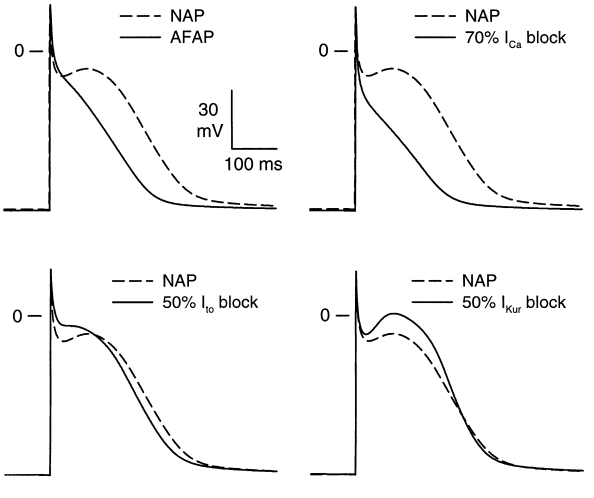

Fig. 4. Role of AF-induced ionic current abnormalities in producing model AFAP morphology. The first panel (top left) presents a comparison of model NAP and AFAP. Successive panels show a comparison between the model NAP and APs with only one of I_{to} (lower left), I_{Kur} (lower right), or $I_{Ca,L}$ (upper right) currents being altered.

presents corresponding experimental data (right panel) taken from the measurements of Boutjidir et al. [9]. Although rate-adaptation of the model NAP is consistent with some experimental data [14,17], the model typically exhibits a smaller decrease in APD_{90} at faster rates (≥ 3 Hz) compared to other experimental recordings (e.g. Refs. [9,16]). However, a comparison of rate-adaptation in the model NAP and AFAP confirms that the model reproduces qualitatively important features of AF-induced remodeling observed in experimental preparations, namely the overall decrease in APD and the reduced extent of rate-adaptation. The changes in APD that accompany changes in stimulation period in the model AFAP are quite similar to the experimental data of Boutjidir et al., but the model NAP exhibits less of a decrease in APD with decreasing stimulation period compared to the experimental data.

3.3. Potassium channel blockade in model NAP and AFAP

We investigated the effect of potassium channel blockade, implemented via a reduction in maximal conductance of specific potassium currents, on morphology and duration of the model NAP and AFAP. We selected as our targets four currents: I_{to} (90% inhibition), I_{Kur} (90% inhibition), I_{Kr} (90% inhibition), I_{Ks} (90% inhibition), and I_{K1} (20% inhibition). Extensive block of I_{K1} compromises the stability of the resting potential in the model, with failure of repolarization or excessive resting potential depolarization occurring for decreases of the inward rectifier greater than 20%. Results are presented with respect to the control values APD_{-60}, corresponding approximately to the ERP, which are 260 ms for the model NAP and 177 ms for the model AFAP (at 1 Hz).

Fig. 6 shows the result of I_{to} inhibition on the NAP and AFAP during pacing at 1 Hz. Inhibition of I_{to} shortens the NAP by 40 ms (15%) and the AFAP by 15 ms (8%). This paradoxical shortening of APD in response to blockade of a repolarizing current (I_{to}) has been observed experimentally [18]. As shown in the upper panels of Fig. 6, inhibition of I_{to} causes a slowing of phase 1 repolarization following the AP upstroke. This is associated with a more positive plateau potential, sustained by a balance between increased $I_{Ca,L}$ and increased I_{Kur} (see middle and bottom panels). The elevated plateau potential allows for greater activation of I_K (compare middle and lower panels) that increases the rate of mid- and late-repolarization, ultimately producing a shorter APD. Thus, a secondary increase in I_K explains the paradoxical AP shortening caused by I_{to} inhibition in both the NAP and AFAP models.

Fig. 7 shows the result of I_{Kr} inhibition on the model APs. Inhibition of I_{Kr} prolongs the NAP by 105 ms (38%) and the AFAP by 60 ms (34%). Inhibition of I_{Ks} (not shown) prolongs the NAP by 32 ms (12%), prolongs the AFAP by 12 ms (7%), and is qualitatively similar to inhibition of I_{Kr} in its effect on the AP. Because I_{Kr} and I_{Ks}

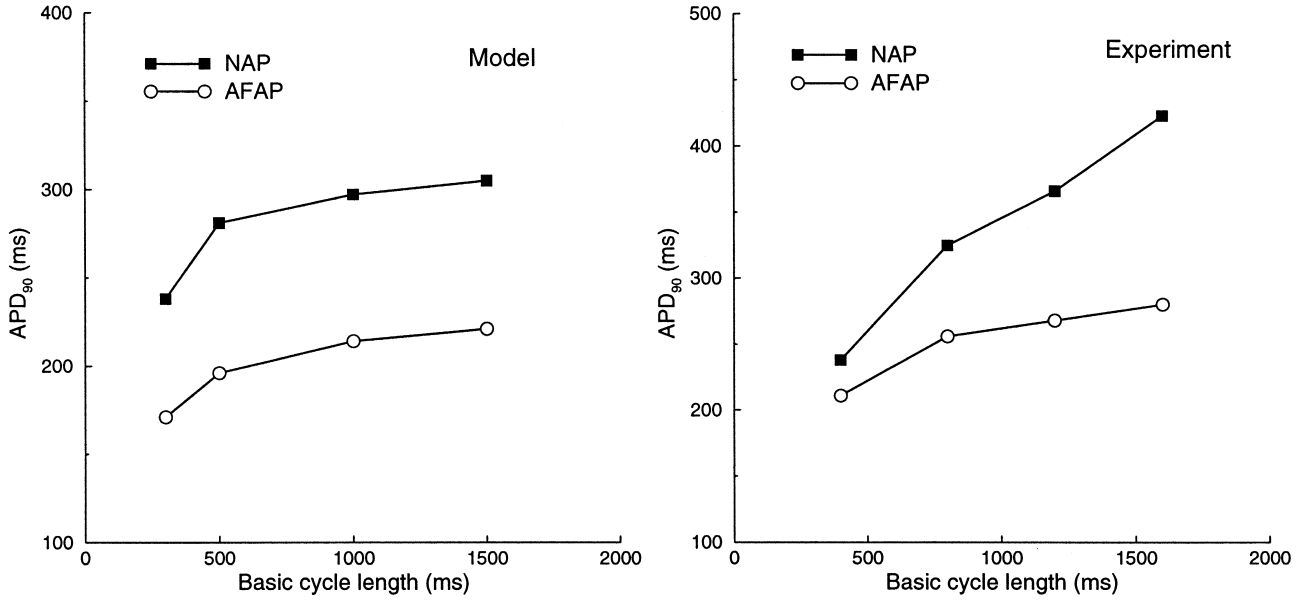

Fig. 5. Relationship between action potential duration (APD_{90}) and basic pacing cycle length (BCL) for the NAP and AFAP. Model simulations yield the curves shown in the left panel. The right panel shows corresponding experimental relationships obtained from an atrial tissue preparation. The graph is based on data from Boutjidir et al. [9].

are activated relatively late during the AP, their inhibition does not disturb the delicate balance of currents during phase 1 repolarization or during the initial phase of the AP plateau (compare middle and lower panels). Inhibition of I_{Kr} or I_{Ks} thus leads to a lengthening of the model NAP and AFAP by slowing the mid- and late-repolarization phases of the AP. Because of its more rapid activation kinetics compared to I_{Ks}, I_{Kr} is more prominent during the AP, which explains the larger effect of I_{Kr} inhibition on both NAP and AFAP.

AP changes resulting from inhibition of I_{Kur} are depicted in Fig. 8. Inhibition of I_{Kur} produces no net change in NAP duration. As depicted in the lower left panel of Fig. 8, following intrinsic I_{to} inactivation, the inhibition of I_{Kur} disturbs the current balance during the plateau, allowing $I_{Ca,L}$ activation to drive the plateau potential well above 0 mV. The more positive plateau voltage leads to increased I_K activation (compare middle and lower left panels), causing an increase in the rate of mid- and late-repolarization. The increase in I_K is able to compensate for the large increase in plateau height and duration, ultimately producing no net change in APD. However, inhibition of I_{Kur} *is* able to lengthen the AFAP by 25 ms (12%). In this case, the lower initial plateau height of the AFAP relative to the NAP limits the increase in $I_{Ca,L}$ and plateau height resulting from I_{Kur} inhibition. The increase in plateau potential occurs over a range (below 0 mV) where the increase in I_K activation is less pronounced. The smaller increase in I_K activation can no longer compensate for the increase in plateau height and duration, and lengthening of the APD is observed. A comparison of our results for the NAP and AFAP suggests that AP prolongation via I_{Kur} inhibition is AF-specific in the model.

Finally, Fig. 9 shows the result of I_{K1} inhibition on the model NAP and AFAP. Inhibition of I_{K1} prolongs the NAP by 25 ms (10%) and the AFAP by 25 ms (14%). As in the case of I_{Kr} inhibition, I_{K1} is active relatively late in the AP and its inhibition does not disturb the balance of currents during phase 1 repolarization or during the plateau phase of the AP (compare middle and lower panels). Inhibition of I_{K1} leads to a lengthening of the model NAP and AFAP by slowing down the late-repolarization phase of the AP.

3.4. Synergy of K^+-current block

Because the effect of I_{Kur} inhibition on NAP duration is limited as a result of increased I_K activation, we postulated that I_{Kr} inhibition could serve to potentiate the effect of I_{Kur} inhibition. We therefore investigated the effect of combined inhibition of I_{Kur} and I_{Kr} on the model NAP and AFAP. Fig. 10 (top panels) shows the result of combined inhibition of I_{Kur} and I_{Kr} (90% for each) on the APs. For the NAP, combined inhibition prolongs APD_{-60} by 132 ms (51%). For the AFAP, combined inhibition prolongs APD_{-60} by 130 ms (73%). On the basis of a purely additive effect, one would predict an APD_{-60} increase of 105 ms for NAP and 85 ms for AFAP. The bar graph of Fig. 10 (lower panel) clearly illustrates how, in both cases, the blocks act synergistically to produce a supra-additive effect on APD. Hence, especially in the case of AFAP, I_{Kr} blockade greatly potentiates the effect of I_{Kur} inhibition on the atrial AP.

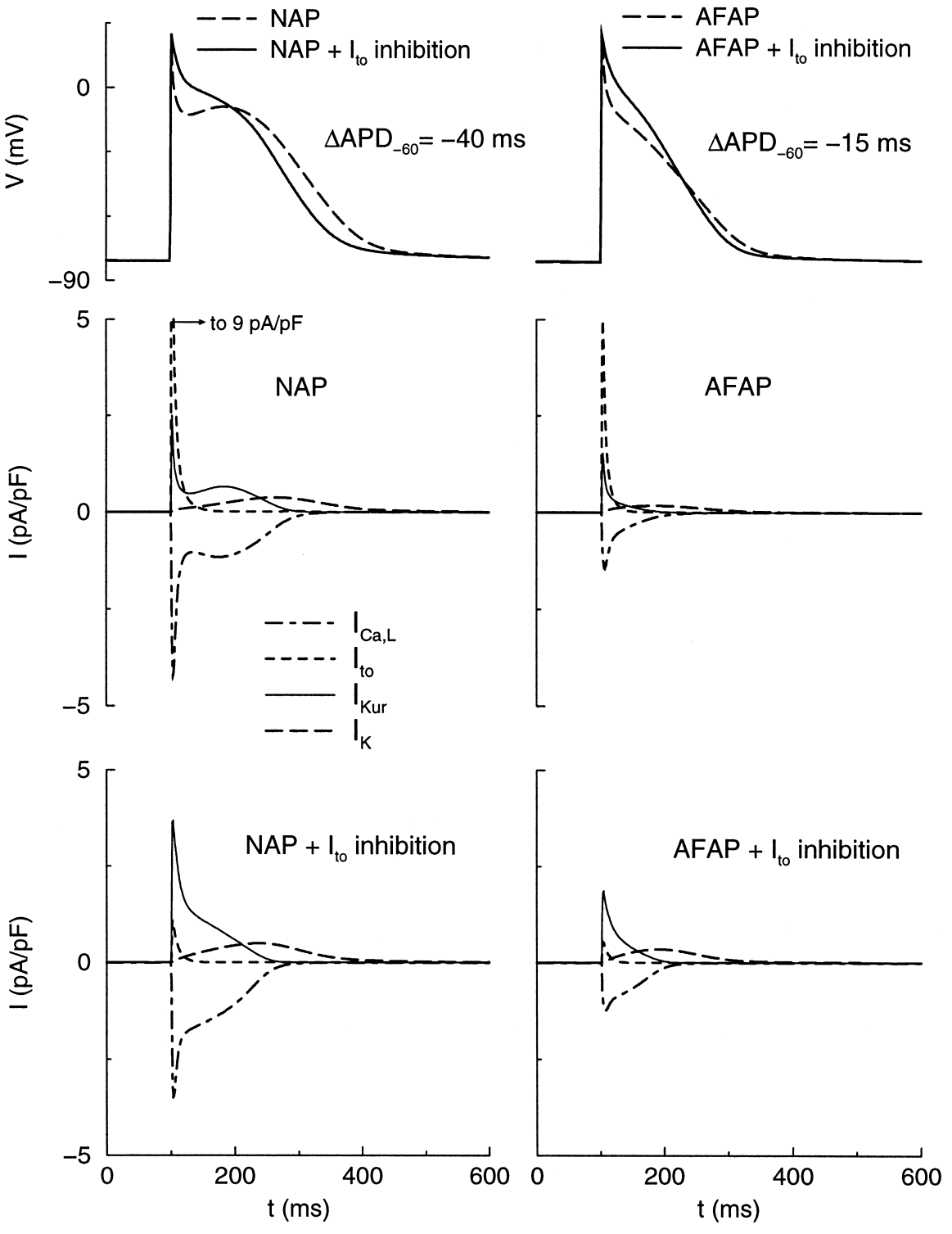

Fig. 6. Effect of I_{to} inhibition (90% reduction in maximal conductance) on model NAP and AFAP. The top panels show the control AP morphologies and the APs after I_{to} inhibition. The net change in APD is given. The lower panels show the evolution of selected membrane currents in the absence or presence of I_{to} inhibition. The NAP I_{to} current peaks off the graph scale at 9 pA/pF, as indicated.

3.5. AP heterogeneity and effects of K^+-current block

We had suggested previously that I_{Kur} might be an attractive target for new antiarrhythmic agents because of its apparent importance in human atrial repolarization [26] and its absence in human ventricle [27]. The results of the model indicate that secondary changes in I_K triggered by the increase in plateau height that accompanies I_{Kur}

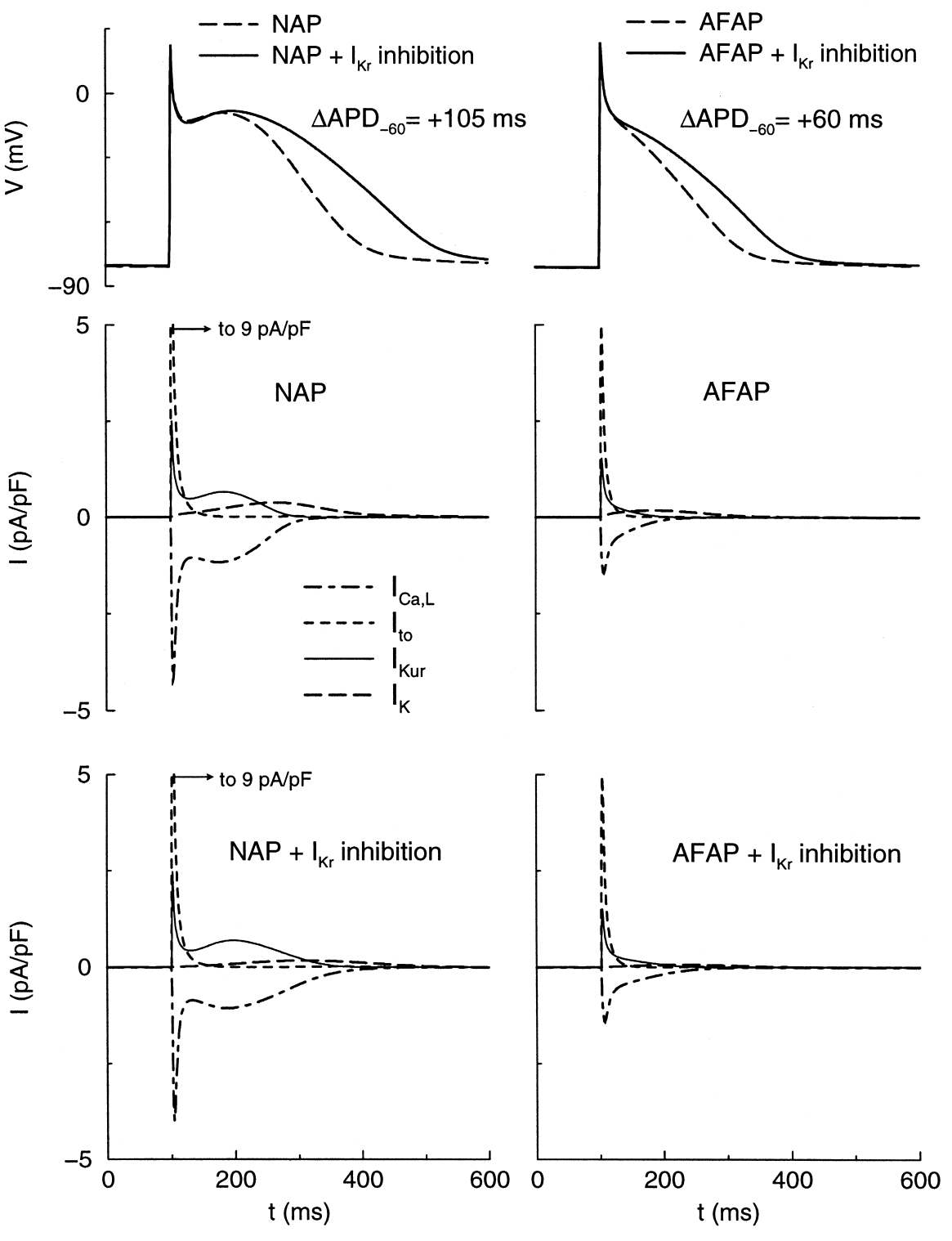

Fig. 7. Effect of I_{Kr} inhibition (90% reduction in maximal conductance) on model NAP and AFAP. The top panels show the control AP morphologies and the APs after I_{Kr} inhibition. The net change in APD is given. The lower panels show the evolution of selected membrane currents in the absence or presence of I_{Kr} inhibition. The NAP I_{to} current peaks off the graph scale at 9 pA/pF, as indicated.

inhibition can result in no net change in NAP duration in response to I_{Kur} block.

The observation of a lack of an effect of I_{Kur} inhibition on NAP duration contrasts with previous experimental evidence for APD prolongation by I_{Kur} inhibition in atrial myocytes from patients in sinus rhythm and without atrial disease [26]. We therefore considered the possibility that AP heterogeneity, as previously described in normal

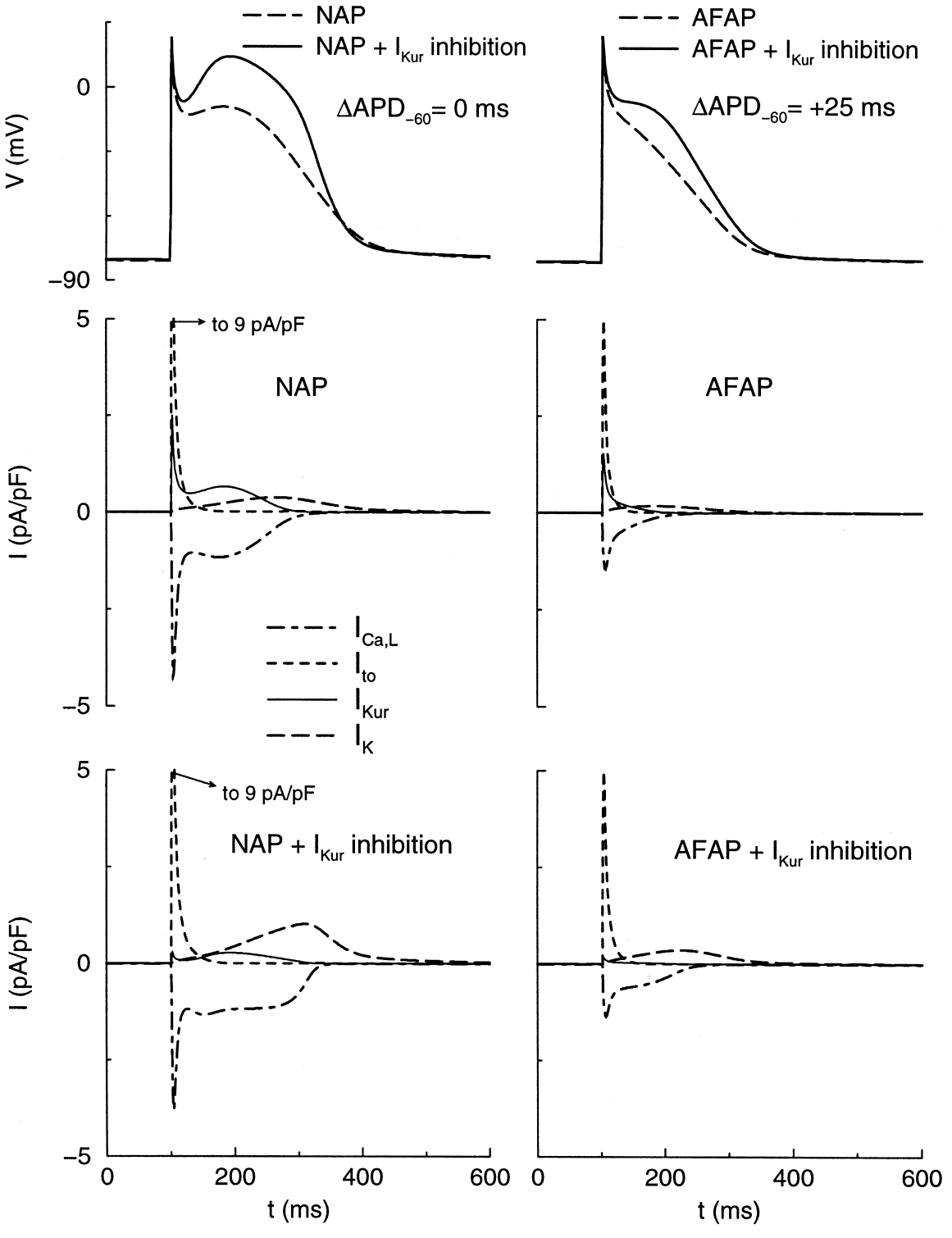

Fig. 8. Effect of I_{Kur} inhibition (90% reduction in maximal conductance) on model NAP and AFAP. The top panels show the control AP morphologies and the APs after I_{Kur} inhibition. The net change in APD is given. The lower panels show the evolution of selected membrane currents in the absence or presence of I_{Kur} inhibition. The NAP I_{to} current peaks off the graph scale at 9 pA/pF, as indicated.

human atrial tissues [19,20], may modify the response to K^+-channel inhibition. The model NAP exhibits a spike-and-dome morphology, typically referred to as a type 2 AP [19]. We modified the model parameters to produce a characteristic rectangular type 1 AP by decreasing the maximal conductance of I_{to} by 70%. A characteristic triangular type 3 AP was produced by decreasing the maximum $I_{Ca,L}$ conductance by 70%. These changes are

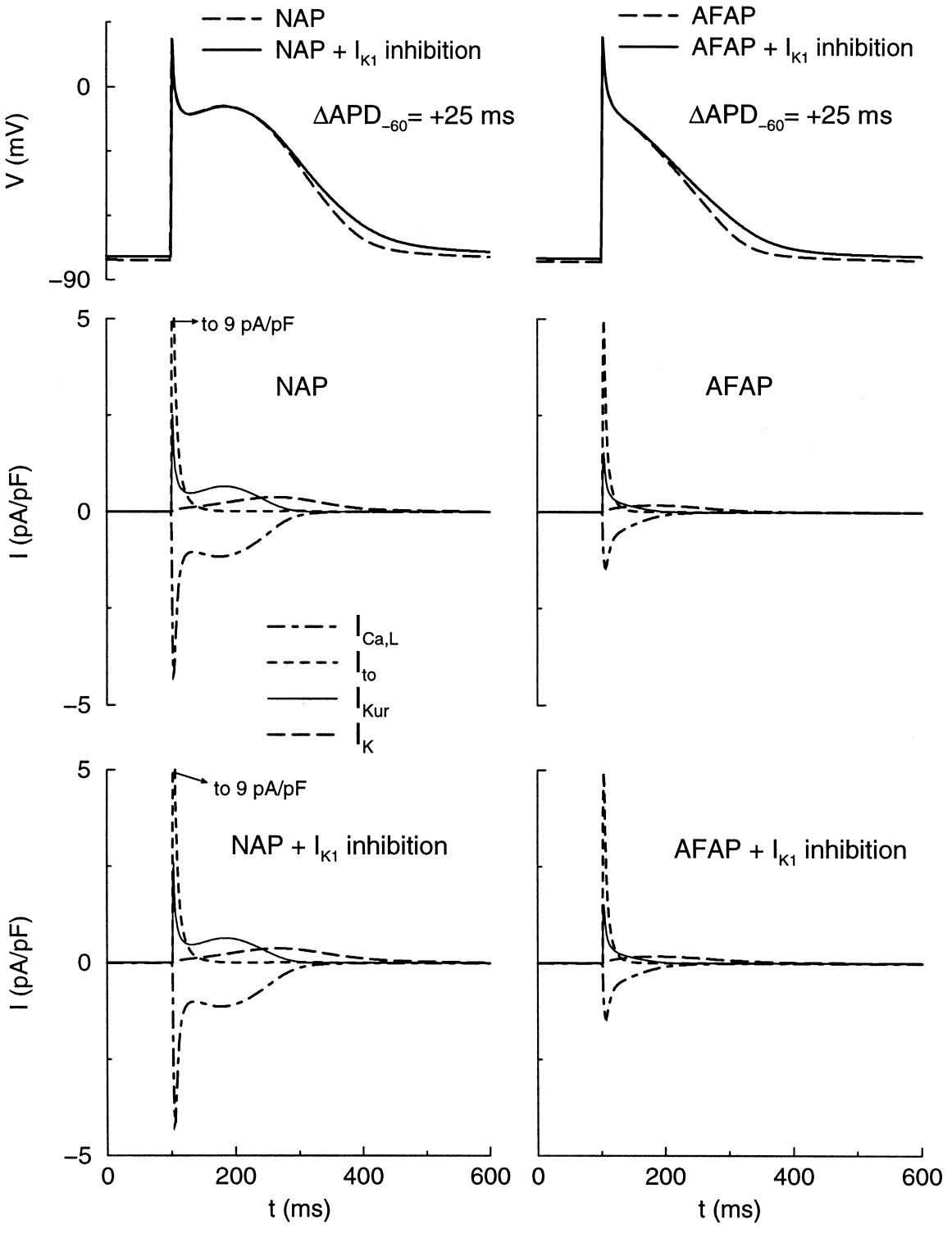

Fig. 9. Effect of I_{K1} inhibition (20% reduction in maximal conductance) on model NAP and AFAP. The top panels show the control AP morphologies and the APs after I_{K1} inhibition. The net change in APD is given. The lower panels show the evolution of selected membrane currents in the absence or presence of I_{K1} inhibition. The NAP I_{to} current peaks off the graph scale at 9 pA/pF, as indicated.

consistent with existing studies of ionic mechanisms of AP heterogeneity [14,21]. The effects of inhibition of various K^+-channels and the three main AP types are shown in Fig. 11. The control APD_{-60} values are 232 ms for the type 1 AP, 260 ms for the type 2 AP, and 149 ms for the type 3 AP. I_{to} inhibition reduces APD in type 1 (10 ms) and type 2 (40 ms) cells, and causes an increase in APD in type 3 cells (13 ms). I_{Kur} inhibition increases APD in type

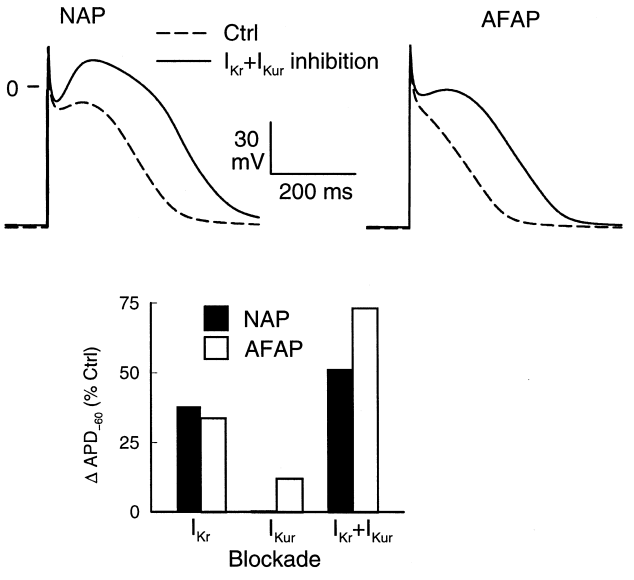

Fig. 10. Effect of combined inhibition (90% each) of I_{Kr} and I_{Kur} on the model NAP and AFAP. Combined inhibition lengthens APD of both NAP (top left panel) and AFAP (top right panel). The lower panel shows that the combined action of I_{Kr} and I_{Kur} inhibition is synergistic, producing an effect much larger than the sum of the effects of the individual channel blockades.

1 (18 ms) and type 3 (27 ms) cells, without affecting APD in type 2 cells. I_{Kr} inhibition increases APD in all cell types, but the increase in type 3 cells (23 ms) is much less than the increase in type 1 (128 ms) or type 2 (105 ms) cells. Combining I_{Kur} and I_{Kr} inhibition strongly increases APD in all cell types (154, 132, and 77 ms in types 1, 2, and 3 cells, respectively). These results indicate that AP morphology may be an important determinant of the effects of K^+-channel inhibition on AP repolarization, even in normal heart.

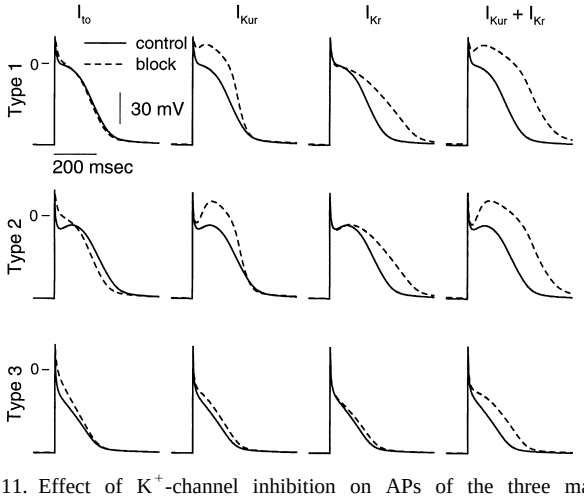

Fig.11. Effect of K^+-channel inhibition on APs of the three main morphological types. Each row shows the results of inhibition of I_{to}, I_{Kur}, I_{Kr}, and I_{Kur}+I_{Kr} for a given AP type. Each column shows the result of inhibition of a specific K^+-channel (or a combination of them) for the three main AP types.

4. Discussion

In this study, we used our recently developed mathematical model of the normal human atrial AP [14] to investigate the effects of AF on the human atrial AP and the results of specific potassium channel inhibition. We found that experimentally determined changes in I_{to}, I_{Kur} and $I_{Ca,L}$ are sufficient to account for the effects of AF on the human AP. We also noted that the overall effects of K^+-channel inhibition on the AP are sensitive to the alterations in other currents that they produce. Channel inhibition can produce different effects on the NAP and AFAP, and combined inhibition of I_{Kur} and I_{Kr} can have synergistic effects on the AP.

We showed that experimentally measured changes in I_{to}, I_{Kur}, and $I_{Ca,L}$ were sufficient, when incorporated in the model, to reproduce the experimental AP morphology changes associated with AF. Most of the change in morphology could be attributed to the decrease in $I_{Ca,L}$; however, the concomitant reductions in I_{to} and I_{Kur} should not be overlooked. The changes in early repolarization and plateau height resulting from reduced I_{to} and I_{Kur} may have important consequences for the response of AF-modified myocytes to pharmacological agents. Our simulations of potassium channel inhibition in the NAP and AFAP models have shown that plateau height can modulate the AP response to channel blockade, as evidenced by the different response of the model NAP and AFAP to I_{Kur} inhibition.

The basis for the reduction in current densities observed as a consequence of AF is not yet resolved. The role of intracellular calcium in electrical remodeling has received much recent attention. Evidence has amassed pointing to calcium overload and a concomitant decrease in inward calcium current as the prominent mechanism contributing to the changes associated with AF. In pig atria, preliminary observations suggest that myocardial calcium concentration are approximately doubled following only 25 min of rapid pacing-induced AF [22]. In acute dog models of rapid pacing-induced AF, atrial biopsy specimens showed mitochondrial swelling, suggesting that tachycardia of the atrial tissue promoted intracellular calcium overload [25]. Whether or not this increase in intracellular calcium is responsible for the downregulation of membrane channel proteins or is directly involved in the inactivation of $I_{Ca,L}$ in AF-remodeled myocytes remains to be determined. Although the model reproduces the short-term changes in intracellular calcium concentration that occur during the AP, long-term modeling of intracellular calcium concentrations over periods of hours of stimulation requires a level of accuracy in the representation of intracellular calcium handling mechanisms that is not yet available.

We have shown that the NAP and AFAP models qualitatively reproduce the rate-adaptation changes associated with AF-induced electrical remodeling. Quantitatively, the model NAP displays rate-adaptation that may be

considered less than average at pacing rates faster than 3 Hz [9,16], but it remains within the range of experimental observations [14,17]. AFAP rate-adaptation agrees with experimental observations showing decreased overall APD at slow rates and decreased relative shortening of APD at fast pacing rates [9,16].

Our investigation of potassium channel blockade has revealed some interesting properties of the NAP and AFAP. In particular, we showed a preferential effect of I_{Kur} inhibition in prolonging AFAP duration without an effect on NAP duration. Hence, I_{Kur} inhibition may be more effective in prolonging ERP in patients with AF. Nygren et al. [15] recently published their own mathematical model of the human atrial AP, in which they discuss the response of the AP to I_{Kur} block. They surmised that AF-remodeled cells with an already reduced I_{Kur} would show a smaller AP prolongation as a result of I_{Kur} block. They based this assumption on the fact that the remodeled cell would should larger relative I_{Kr} compared to control, and that this would accentuate the paradoxical shortening effect associated with I_{Kr} recruitment upon block of I_{Kur}. This would hold true if I_{Kur} were the only current modified as a result of AF-induced remodeling. However, the concomitant reduction in $I_{Ca,L}$ lowers the plateau to such an extent that the result is a net decrease in I_{Kr} recruitment upon I_{Kur} block. We have also shown that combined inhibition of I_{Kur} and I_{Kr} can produce a supra-additive effect, with I_{Kr} inhibition acting to potentiate the limited effect of I_{Kur} on APD. This synergistic effect is more important in AFAP compared to NAP. Both findings suggest potentially interesting approaches for the development of AF-specific drug therapies. The results of the present analysis point to a selectivity of I_{Kur} inhibition for prolonging the AFAP, which may prove to be a desirable property.

Further work is necessary to evaluate the contributions of AP heterogeneity, AP activation rate, and drugs to the overall response of atrial tissue in both normal and AF conditions. In particular, interesting phenomena related to frequency-dependence or use-dependence of channel blockers certainly beg investigation using our model. Those results should depend sensitively on the accuracy of potassium current kinetics in our model, especially for the delayed rectifier current. Our formulation of the rapid and slow components of I_K is a compromise between accuracy and computational tractability. The model does not reproduce certain critical aspects of I_{Kr} and I_{Ks}, including the different activation and deactivation kinetics at certain voltages. These properties would play a significant role in the AP response to channel blockade at the fast rates typical of AF. Furthermore, there are important discrepancies in the literature regarding the relative rates of I_{Kr} and I_{Ks} deactivation [23,24]. Additional experimental data is needed to develop a more detailed formulation of I_K that would allow accurate modelling of the frequency-dependent effects of I_K inhibition.

Our analysis suggests a potentially important role of AP heterogeneity in determining the effects of blocking specific K^+-channels. Relatively little is known about the determinants and mechanisms of AP heterogeneity among and within different atrial regions; however, experimental data suggest that it may be an important determinant of AF [11,28]. Further experimental and modeling work are needed to explore the nature, mechanisms and consequences of atrial AP heterogeneity for the occurrence of AF, the effects of atrial remodeling, and the actions of antiarrhythmic drugs.

Acknowledgements

Supported by grants from the Medical Research Council of Canada, the Natural Sciences and Engineering Research Council of Canada, the Heart and Stroke Foundation of Quebec and the Fonds de Recherche de l'Institut de Cardiologie de Montréal. Dr. Courtemanche is a Research Scholar of the Fonds de Recherche en Santé du Québec.

References

[1] Wijffels MCEF, Kirchhof CJHJ, Dorland R, Allessie MA. Atrial fibrillation begets atrial fibrillation: a study in awake chronically instrumented goats. Circulation 1995;92:1954–1968.

[2] Wijffels MCEF, Kirchhof CJ, Dorland R, Power J, Allessie MA. Electrical remodeling due to atrial fibrillation in chronically instrumented conscious goats: roles of neurohumoral changes, ischemia, atrial stretch, and high rate of electrical activation. Circulation 1997;96(10):3710–3720.

[3] Wijffels MCEF, Kirchhof CJHJ, Dorland R, Allessie MA. Electrical remodeling due to atrial fibrillation. In: Allessie MA, Fromer M, editors, Atrial and Ventricular Fibrillation: Mechanisms and Device Therapy, Futura Publishing Co, Armonk, NY, 1997, pp. 215–232.

[4] Morillo CA, Klein GJ, Jones DL, Guiraudon CM. Chronic rapid atrial pacing. Structural, functional, and electrophysiological characteristics of a new model of sustained atrial fibrillation. Circulation 1995;91(5):1588–1595.

[5] Elvan A, Wylie K, Zipes DP. Pacing-induced chronic atrial fibrillation impairs sinus node function in dogs. Electrophysiological remodeling. Circulation 1996;94(11):2953–2960.

[6] Gaspo R, Bosch RF, Talajic M, Nattel S. Functional mechanisms underlying tachycardia-induced sustained atrial fibrillation in a chronic dog model. Circulation 1997;96(11):4027–4035.

[7] Tieleman RG, De Langen CDJ, Van Gelder IC et al. Verapamil reduces tachycardia-induced electrical remodeling of the atria. Circulation 1997;95:1945–1953.

[8] Yue L, Feng J, Gaspo R et al. Ionic remodeling underlying action potential changes in a canine model of atrial fibrillation. Circ Res 1997;81(4):512–525.

[9] Boutjidir M, LeHeuzey JY, Lavergne T et al. Inhomogeneity of cellular refractoriness in human atrium: Factor of arrhythmia? PACE 1986;9:1095–1100.

[10] Van Wagoner DR, Pond AL, McCarthy PM, Trimmer JS, Nerbonne JN. Outward K^+ current densities and Kv1.5 expression are reduced in chronic human atrial fibrillation. Circ Res 1997;80:772–781.

[11] Fareh S, Villemaire C, Nattel S. Importance of refractoriness heterogeneity in the enhanced vulnerability to atrial fibrillation induction caused by tachycardia-induced atrial electrical remodeling. Circulation 1998;98:2202–2209.

[12] Attuel P, Childers R, Cauchemez B et al. Failure in the rate adaptation of the atrial refractory period: its relationship to vulnerability. Int J Cardiol 1982;2:179–197.
[13] Van Wagoner DR, Lamorgese M, Kirian P et al. Calcium current density is reduced in atrial myocytes isolated from patients in chronic atrial fibrillation (abstract). Circulation 1997;96(8):I-180.
[14] Courtemanche M, Ramirez RJ, Nattel S. Ionic mechanisms underlying human atrial action potential properties: Insights from a mathematical model. Am J Physiol 1998;275:H301–H321.
[15] Nygren A, Fiset C, Firek L et al. Mathematical model of an adult human atrial cell: the role of K+ currents in repolarization. Circ Res 1998;82:63–81.
[16] Franz MR, Karasik PL, Li C, Moubarak J, Chavez M. Electrical remodeling of the human atrium: similar effects in patients with chronic atrial fibrillation and atrial flutter. J Am Coll Cardiol 1997;30(7):1785–1792.
[17] Wang Z, Pelletier LC, Taljic M, Nattel S. Effects of flecainidine and quinidine on human atrial action potentials: Role of rate-dependence and comparison with guinea pig, rabbit and dog tissues. Circulation 1990;82:274–283.
[18] Shibata EF, Drury T, Refsum H, Aldrete V, Giles W. Contributions of a transient outward current to repolarization in human atrium. Am J Physiol 1989;257:H1773–H1781.
[19] Wang Z, Fermini B, Nattel S. Delayed rectifier outward current and repolarization in human atrial myocytes. Circ Res 1993;73:276–285.
[20] Benardeau A, Hatem SN, Rucker-Martin C, et al. Contribution of Na^+/Ca^{2+} exchange to action potential of human atrial myocytes. Am J Physiol 1996;271 (Heart Circ Physiol 1996;40):H1151–H1161.
[21] Feng J, Yue L, Wang Z, Nattel S. Ionic mechanisms of regional action potential heterogeneity in canine right atrium. Circ Res 1998;83:541–551.
[22] Leistad E, Verburg E, Christensen G. Cytosolic calcium overload, not atrial ischemia,accounts for post-fibrillation atrial dysfunction. Circulation 1994;90:I–492.
[23] Sanguinetti MC, Jurkiewicz NK. Delayed rectifier outward K^+ current is composed of two currents in guinea pig atrial cells. Am J Physiol 1991;260 (Heart Circ Physiol 1991;29):H393–H399.
[24] Heath BM, Terrar DA. The deactivation kinetics of the delayed rectifier components I_{Kr} and I_{Ks} in guinea-pig isolated ventricular myocytes. Exp Physiol 1996;81:605–621.
[25] Goette A, Honeycutt C, Langberg JJ. Electrical remodeling in atrial fibrillation: Time course and mechanisms. Circulation 1996;94:2968–2974.
[26] Wang Z, Fermini B, Nattel S. Sustained depolarization-induced outward current in human atrial myocytes: evidence for a novel delayed rectifier potassium current similar to Kv1.5 cloned channel currents. Circ Res 1993;73:1061–1076.
[27] Li GR, Feng J, Yue L, Carrier M, Nattel S. Evidence for two components of delayed rectifier K^+ current in human ventricular myocytes. Circ Res 1996;78:689–696.
[28] Liu L, Nattel S. Differing sympathetic and vagal effects on atrial fibrillation in dogs: role of refractoriness heterogeneity. Am J Physiol 1997;273:H805–H816.